China Geology 6 (2023) 252−268

China Geology

Journal homepage: http://chinageology.cgs.cn
https://www.sciencedirect.com/journal/china-geology

Mineralization of the Liwu large-scale stratiform copper deposits in Sichuan Province, China: Constraints from fluid inclusions

Hua-yun Yuan[a], Qing Zhou[b,*], Yuan-bao Song[a], Wei Zhang[a], Hui-hua Zhang[b], Tong-zhu Li[b], Tao Yin[a], Chang-nan Wang[c], Gao-lin Tang[c]

[a] *Evaluation and Utilization of Strategic Rare Metals and Rare Earth Resource Key Laboratory of Sichuan Province, Sichuan Geological Survey, Chengdu* 610081, *China*
[b] *Chengdu Center, China Geological Survey, Ministry of Natural Resources, Chengdu* 610081, *China*
[c] *Sichuan Liwu Copper Mining Company, Ganzi* 626200, *China*

ARTICLE INFO

Article history:
Received 20 October 2022
Received in revised form 23 January 2023
Accepted 8 February 2023
Available online 14 April 2023

Keywords:
Stratiform copper deposit
Mineralization
Fluid inclusion
H-O isotopes
Hydrothermal deposit
Dome structure
Middle Proterozoic metamorphic rock
Mineral exploration engineering
Sichuan Province

ABSTRACT

The Liwu stratiform copper deposit is located in the northwestern Jianglang dome, western China. Current studies mainly focus on the genetic type and mineralization of this deposit. Detailed fluid inclusion characteristics of metallogenic period quartz veins were studied to reveal the ore-forming fluid features. Laser Raman analysis indicates that the ore-forming fluids is a H_2O-NaCl-CH_4 (-CO_2) system. Fluid inclusions microthermometry shows a homogenization temperature of 181–375°C and a salinity of 5.26%–16.99% for the disseminated-banded Cu-Zn mineralization; but a homogenization temperature of 142–343°C and a salinity of 5.41%–21.19% for the massive-veined Cu-Zn mineralization. These features suggest a medium–high temperature and a medium salinity for the ore-forming fluids. H-O isotopic data indicates that the ore-forming fluids were mainly from the metamorphic and magmatic water, plus minor formation water. And sulfur isotopic data indicates that sulfur was mainly derived from the formation and magmatic rocks. Metallogenesis of the disseminated-banded mineralization was mainly correlated with fluid mixing and water-rock reaction; whereas that of the massive-veined mineralization was mainly correlated with fluid boiling. The genetic type of the deposit is a medium-high temperature hydrothermal deposit related to magmatism and controlled by shear zones. This study is beneficial to understand the stratiform copper deposit.

1. Introduction

The Liwu copper deposit is located in the northwestern Jianglang dome in the western China. It is a large-scale medium-high temperature hydrothermal deposit related to magmatism and controlled by shear zones. The deposit contains more than 0.8 ×10^6 t of Cu, 0.5 ×10^6 t of Zn, 133 t of Ag and 1300 t of Co. The deposit has an average Cu grade of 0.51%–2.50%, an average Zn grade of 0.29%–1.64%, an average Ag grade of 10×10^{-6}–46×10^{-6} and an average Co grade of more than 0.01% (Zhou Q et al., 2017).

The Liwu copper-rich deposit is composed of several ore blocks, such as Liwu, Heiniudong, Zhongzui, Wajingou, Baixianglin and Sunyelin, which are produced around the Mesoproterozoic dome structure and their distribution is controlled by the dome structure (Fig. 1). The dome core is the metamorphic rocks of the Mesoproterozoic Liwu Group, the mantle part is the metamorphic rocks of the Paleozoic Jianglang Formation, Jiaba Formation and Wulaxi Formation, and the cap bed is the flysch construction of the Mesozoic Xikang Group. The Liwu copper deposit is located in the Liwu Group in the core of dome structure and has the characteristics of producing along the stratum (Hu RQ et al., 2018; Fig. 2).

The deposit have been extensively studied for decades; however, controversies still exist on its genetic type and metallogenesis. In terms of sources of ore-forming materials, some scholars believe that ore-forming materials mainly come from volcanic sediments and sedimentary rocks (Yao JD, 1990; Song TH and Xing SC, 1990; Yan DP et al., 2003; Yao P et al., 2008), while others suggest that they are mainly from intrusive magma (Feng XL et al., 2008; Chen MH et al.,

First author: *E-mail address*: csuyhy@163.com (Hua-yun Yuan).

* Corresponding author: *E-mail address*: zhouq556@163.com (Qing Zhou).

Literary editor: Jie Meng
doi:10.31035/cg2023034
2096-5192/© 2023 China Geology Editorial Office.

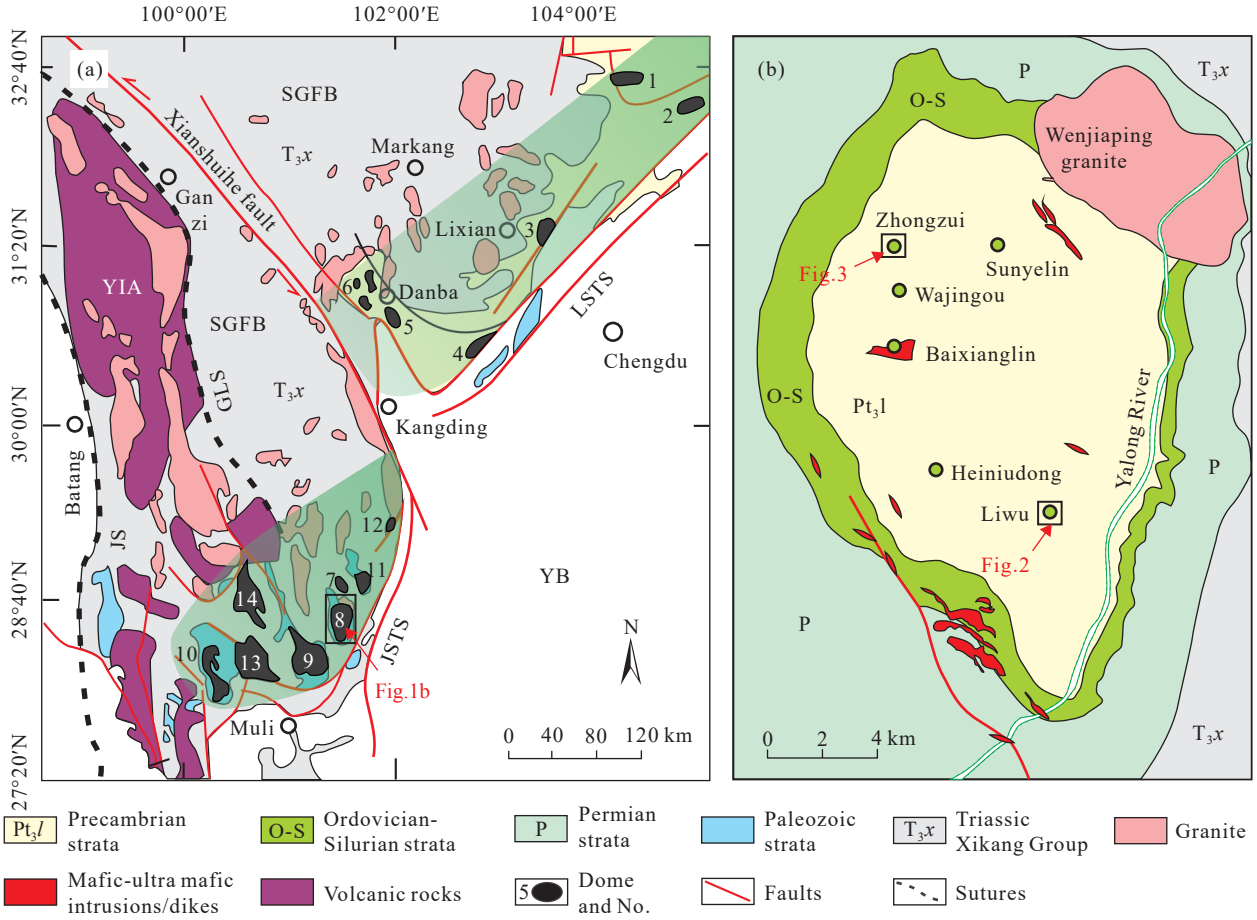

Fig. 1. Regional geological maps showing the Songpan–Ganzi fold belt (SGFB) (a) and the distributions of the Liwu copper deposit in the Jianglang dome (b) (after Zhou Q et al., 2017). 1–Motianlin; 2–Jiaoziding; 3–Xuelongbao; 4–Yaside; 5–Gezong; 6–Gongchai; 7–Taka; 8–Jianglang; 9–Changqiang; 10–Qiasi; 11–Sanya; 12–Tianwan;13–Wachang; 14–Tangyang. Abbreviations: YB–Yangtze Block; SGFB–Songpan–Ganzi fold belt; LSTS–Longmenshan thrust system; JSTS–Jinpingshan thrust system; YIA–Yidun island arc; GLS–Ganzi–Litang suture. Circles with dashed lines represent the targeting area of copper polymetallic deposits in the eastern SGFB.

2013). In terms of ore-forming fluid, some scholars believe that it mainly comes from the mixture of metamorphic water and atmospheric precipitation (Yan DP et al., 2003), some believe that it is the mixture of seawater, basin water and metamorphic water (Li JZ et al., 2012), and some believe that it is mainly magmatic water and metamorphic water, mixed seawater and atmospheric precipitation (Feng XL et al., 2008; Chen MH et al., 2013), and others suggest that it is a mixture of magmatic water and atmospheric precipitation (Song TH and Xing SC, 1990).

In addition, the origin of the deposit is particularly hotly debated. Some scholars classified the deposit as a volcanogenic massive sulfide deposit (Yao JD et al., 1990), or its metamorphic modified deposits (Yao P et al., 2008; Li JZ et al., 2012). Others believe that the deposit is a high temperature hydrothermal filling metasomatic deposit associated with acidic magmatic activity (Song TH and Xing SC, 1990), or a medium-high temperature hydrothermal deposit associated with orogenic activity (Yan DP et al., 2003). Zhou Q et al. (2017) studied the Re–Os dating of chalcopyrite and found that the copper mineralization age of the deposit (about 151.1±4.8 Ma) was slightly later than that of the local Wenjiaping granite (about 160.9±1.0 Ma–161.52±0.62 Ma). Combined with the data of Pb isotope of chalcopyrite, B isotope of tourmaline and Pb isotope of granite, it is suggested that the deposit may be related to coeval felsic magmatism.

Ore-forming fluid is a key to constrain the source, migration, accumulation and metallogenesis of ore deposits. Fluid inclusions are "probes" or "fossils" to record the activity of ore-forming fluids and study fluid mineralization (Chen YJ et al., 2007). It is one of the main purposes of studying fluid inclusions to explain and reveal various geological processes such as fluid migration and fluid mineralization through qualitative and quantitative analysis of paleofluid in the inclusions (Lu HZ and Guo DJ, 2000). Routine studies of fluid inclusions include petrographic studies, temperature and composition tests, and calculations of fluid salinity, pressure, and redox degree based on them. The fluid composition in inclusions can be used to trace the source, migration channel and evolution of the ore-forming fluid system (Ghazi AM et al., 1994; Chen BL et al., 1999; Lu HZ et al., 1999).

Previous studies have reported the ore-forming fluids for the Liwu copper deposit. However, the source of ore-forming fluid is still controversial， and there are still some problems in the research of the ore-forming fluids. Firstly, the previous

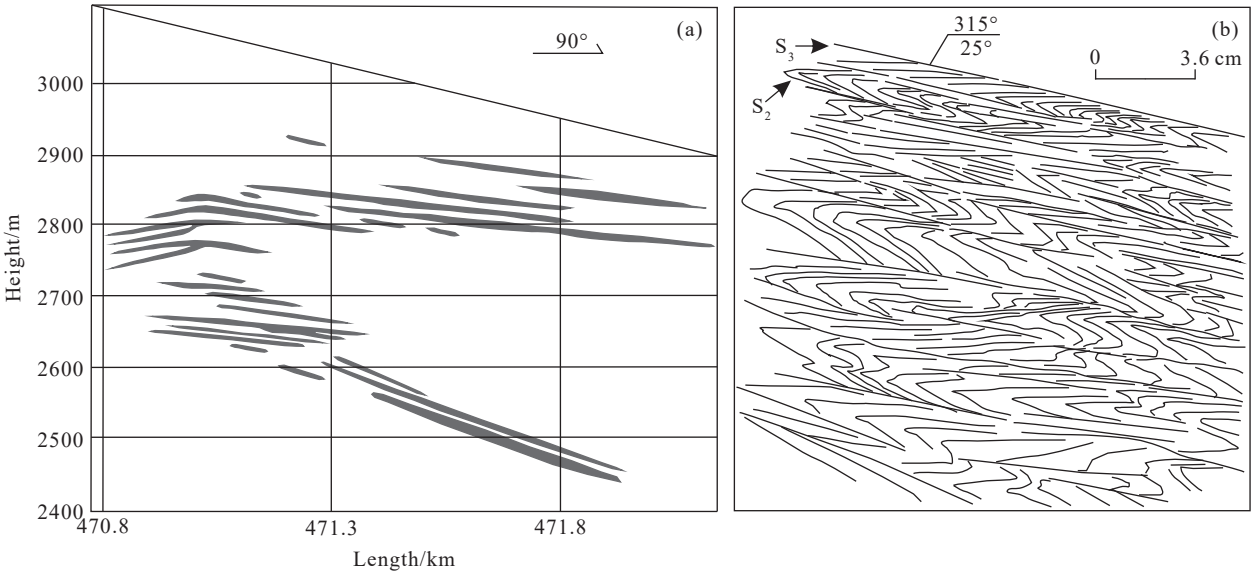

Fig. 2. Longitudinal projection of the ore body of the Liwu copper deposit (a, after Hu RQ et al., 2018) and metamorphic deformation of rocks in the Liwu Group (b, after Zhang HH et al., 2013). The ore body develops along the fold deformation stratum in (a), and the overall morphology of the ore body is similar to the rock deformation morphology of Liwu Group in (b)

studies often ignored the features and composition of the fluid inclusions to help determine the source of the fluid. The source of fluids can be accurately judged by synthesizing multiple methods (Wang ZC et al., 2010; Guo CY et al., 2011). The fluid composition in the inclusions often plays an important role in studying the evolution of fluid system and tracing the origin of fluid (Lu HZ et al., 1999; Lu HZ and Guo DJ, 2000). In addition, rare earth trace element characteristics are often employed to reveal the source of ore-forming fluids and minerals. Secondly, previous studies on fluid mainly focused on fluid inclusions in ore-bearing veins near the massive ore bodies. However, there is a lack of systematic research on the classification and stages of ore-forming fluids. Chen YJ et al. (2007) believed that a large amount of atmospheric precipitation was often added into fluids at the late stage of mineralization, and only fluids at the early stage could accurately indicate the genesis of ore deposits. It can be seen that the mineralization stage division and systematic study of ore-forming fluids are significant to reveal properties, genesis and evolution of the ore-forming fluids. Therefore, it is still necessary to carry out systematic studies on the ore-forming fluids of the Liwu copper deposits.

On the basis of previous studies, the metallogenic stage was divided by detailed geological survey of the Liwu copper deposit in this paper. Microthermometry and composition analysis of fluid inclusions were further carried out. In addition, the source and evolution of ore-forming fluids, and the migration and precipitation mechanism of copper in the Liwu deposit were detailedly summarized and studied. This study is beneficial to understand the stratiform copper deposit related to shear zones.

2. Geological setting

The Jianglang dome is located among the western Yangtze Block, the southeastern Songpan–Ganzi Orogen and the northwest NE-directed Muli–Jinping arc thrust belt (Fig. 1). The Muli–Jinpingshan arc thrust belt is distributed from north to south, the Jinpingshan thrust belt strikes NE (20°–30°) and its front edge is the Jinpingshan–Xiaojinhe main thrust fault zone. Along the northwest trailing edge of the thrust belt, from north to south, there occurs a series of NNW–SN-trending metamorphic domes, including Sanya, Taka, Jianglang, Changqiang, Wachang, Qiasi, etc.

The Songpan–Ganzi orogenic belt is located between the Yangtze Block and the Paleo-Tethys Orogen. It was formed on the basis of the western passive continental margin of the Yangtze Block through multiple tectonic movements since the Indosinian period. Intracontinental collision-orogeny was continuing since the Yanshanian period, resulting in strong intracontinental compression and convergence. This process prompted the Songpan–Ganzi Orogen to push toward the Yangtze Block from the north and northwest. Finally, the Muli–Jinpingshan large arc-shaped thrust structure was formed. The whole tectonic evolution caused a series of tectonic-magmatic-thermal events such as deformation and metamorphism of the Jianglang dome, magmatic intrusion dome-forming and related Cu poly-metallic mineralization.

The Jianglang dome is a NNW-trending short-axis anticline, with a length of about 25 km, a width of about 20 km and a distribution area of about 500 km^2. Generally, the exposed strata gradually become newer from the inside to the outside, and some strata are lost. The exposed strata are the Liwu Group, Jianglang Formation, Jiaba Formation, Wulaxi Formation and Xikang Group. The Liwu Group is an important ore-bearing layer in the inner dome. Around the Liwu Group in the dome, there are many copper ore blocks, such as Liwu, Haidigou, Heiniudong, Boxianglin, Wajingou, Zhongzui, and Sunyelin. Bedding ductile shear zones are widely developed in the Liwu Group, ranging from a few

centimeters to tens of meters in thickness. The shear zones are closely related to alteration and mineralization. The faults in the area include a thrust on the southern margin of the dome, a left-lateral strike-slip fault in the north-west direction, and a Jinpingshan high-angle thrust on the east side of the dome.

The magmatic rocks in this area are mainly basic volcanic rocks, basic–ultrabasic intrusive rocks and granites. These mafic rocks are widely distributed in the dome, with strong metamorphism and deformation. The granite mainly occurs at Wenjiaping in the northeast of the dome (Liu J et al., 2022).

3. Deposit geology

3.1. Mining geology

The Liwu deposit consists of the Liwu, Heiniudong, Zhongzui, Wajingou, Baixianglin and Sunyelin ore blocks. These ore blocks have similar geological features. In this paper, the mining geology is described with the example of the Zhongzui ore block, where the main samples are collected. The Zhongzui ore block is located in the northwestern Jianglang dome, adjacent to the Wajingou and Baixianglin ore blocks. The exposed strata in the mine area is the Liwu Group (Fig. 3), which has undergone multiple periods of deformation and metamorphism, and the degree of metamorphism can reach the epidote amphibolite facies. The Liwu Group is composed of mica-quartzite, quartzite, garnet-mica-quartz schist, mica schist and (mica) hornblende schist. The different lithological bands in the area often rapidly pinch out or appear laterally.

The regional main period foliation S_3 of the mining area is generally a monoclinic structure with a northwest trending inclination, with a dip of 300°–10° and a dip angle of 20°–50°. In the area, the closed folds and the rootless folds develop along the layers.

There are four large-scale ductile shear belts in the Zhongzui mining area from east to west and from bottom to top. The shear belt forms the current foliation S_4, which is parallel to the occurrence of the regional main period foliation S_3, with a northwest trending inclination and a dip angle of 30°–45°. When the shear belt extends to the northeast, the dip angle tends to become smaller, reaching 20°–30°. The shear belt is mainly expressed in the form of ductile shear

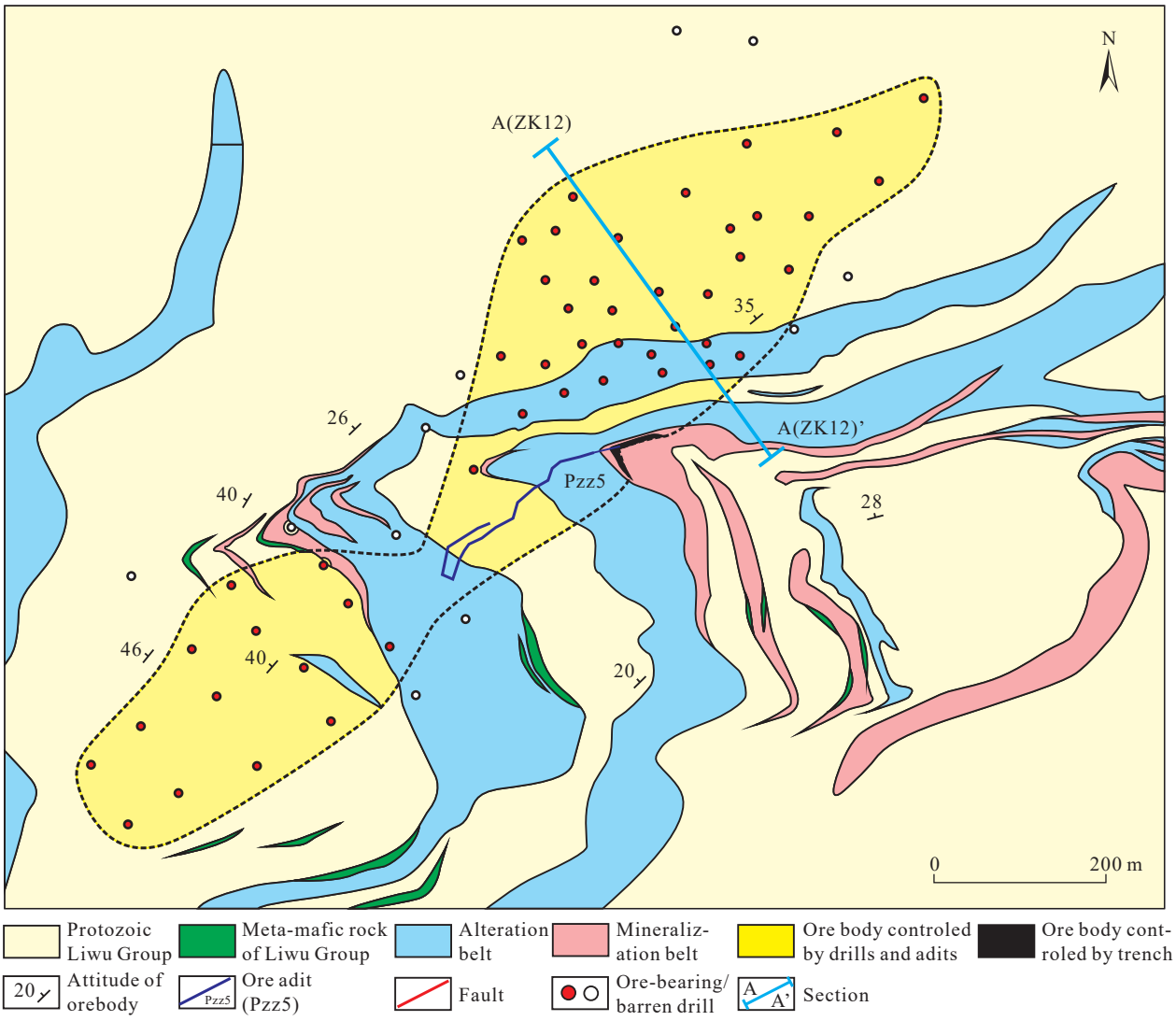

Fig. 3. Geological map of the Zhongzui ore bolck in the Liwu copper deposit (modified from Zhou Q et al., 2017) .

deformation, interlayer fracture and interlayer sliding surface groups. It is the main structure controlling the ore body shape, occurrence, scale and mineralization enrichment. Alteration minerals and metal sulfides often develop along the foliation S_4 formed by shearing, forming mineralized alteration zones or disseminated-banded ore bodies, while massive rich ore bodies occur in the interlayer fracture zone within the shear belt. There are two fractures after the metallogenic period in the northeast of the mining area, which are small in scale and have little damage to the ore body.

The magmatic rocks distributed in the area are mainly some metamorphic basic (volcanic) rocks, which are distributed along regional foliation S_3 in the form of layered or lenticular bands, and often pinch out or appear quickly laterally. The exposed width is tens of centimeters to tens of meters, and the length is several meters to tens of meters, and some of the more stable ones can reach more than 300 m. The vertical apparent thickness of metamorphic basic (volcanic) rock in the borehole are mostly 1–4 m, and some are 5–8 m. The lithology is mainly amphibolite, the original rock of which is some basic volcanic rocks and basic intrusive rocks.

3.2. Ore bodies

The mining area mainly includes two ore bodies, including Z_{1-3} and Z_{1-2} (Fig. 4). Z_{1-3} is located in the west of the mining area, and Z_{1-2} is located in the east of the mining area. The ore bodies are controlled by the ductile shear belt, which are generally stratiform. Their occurrence is commonly parallel to the current foliation of the ore-hosting rocks, and locally crosscuts the current foliation. The strike of ore bodies is 300°–330°, with a northwestern dip, and the two ore bodies

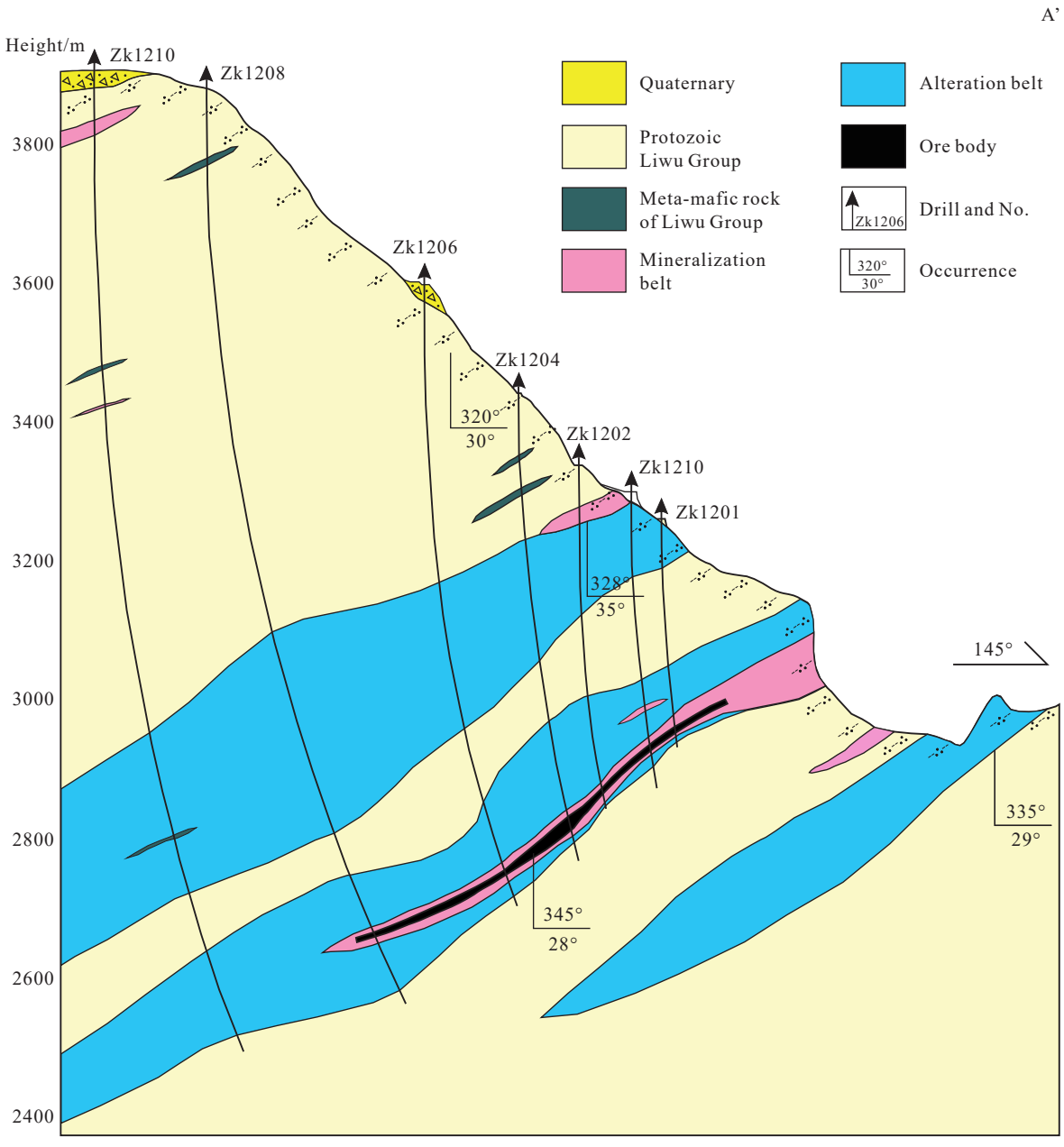

Fig. 4. Cross-section of the Zhongzui ore block in the Liwu deposit. Location of A–A' is shown in Fig. 3.

are roughly in the same horizon.

The Z_{1-3} ore body is semi-concealed, with an exposed length of more than 100 m. The dip angle of the ore body varies from 15° to 40°. The strike length of ore body is 1430 m on horizontal projection, the dip length is mostly 250–563 m, and the control elevation is 2716.47 m to 3130.65 m. The ore body extends steadily and continuously along strike and dip, with a thickness of 0.66–12.83 m, with an average thickness of 4.70 m. Copper content of the ore body is 0.22%–7.27%, with an average of 1.44%; zinc content is 0.03%–4.62%, with an average of 0.67%.

The Z_{1-2} ore body is concealed. The dip angle of the ore body varies from 8°to 31°. The strike length of the ore body is 580 m, the dip length is mostly 230–367 m, and the control elevation is 2974–3166 m. The ore body extends steadily and continuously along strike and dip, with a thickness of 0.96–3.13 m, with an average thickness of 1.63 m. Copper content of the ore body is 0.10%–2.12%, with an average of 0.66%; zinc content is 0.00%–2.94%, with an average of 0.59%.

3.3. Ore structures

The types of the sulfide ores in the deposit include massive ore, brecciated ore, disseminated-banded ore, metal sulfide network vein ore and (tourmaline) quartz vein ore (Fig. 5). The primary metallic minerals in the deposit are mainly pyrrhotite, chalcopyrite and sphalerite, followed by pyrite, ilmenite, and occasionally galena, chalcocite and arsenopyrite. Secondary metal minerals can only be seen in the surface oxidation zone, are mainly limonite, azurite, malachite and various sulfate vitriol minerals. There are small amounts of magnetite and ilmenite in the amphibolite. The gangue minerals mainly consist of quartz, biotite, muscovite, sericite, chlorite, followed by amphibole, garnet, tourmaline, phillips and calcite. The ore structure includes euhedral granular structure, anhedral granular structure, solid-exsolution separation structure, metasomatic erosion structure, metasomatic residual structure, stockwork structure, interstitial structure, ring structure, inclusion structure, etc (Fig. 6).

3.4. Wall rock alteration

Hydrothermal alteration widely occurs in the mining area, and is spatially related to mineralization and shear belts. Ore bodies or mineralization occur in the alteration zone, which generally distributes in the brittle-ductile shear belts. The alteration belt shows a large scale, with several hundred meters in width and more than one hundred meters in thickness. The wall rock alteration is silicification-tourmalinization-staurolite-garnet alteration at early stage, and biotitization-sericitization-chloritization at late stage. The late alteration is superimposed on the early one, and the alteration zoning is not obvious.

There are three stages of garnet alteration. At the early stage, garnets are distributed in elongated bands along the current foliation. At the middle stage, garnet grains are larger and not elongated, and are filled with metal sulfides in the cracks regularly. In the late stage, the garnets are complete and fine grained. The silicification is mainly manifested as recrystallized quartz particles. Quartz bands were formed from the ductile shear deformation, whereas quartz veins filled along or crosscut the current foliation. Biotite, sericite, chlorite and other slim minerals are distributed in various forms, which can be distributed in fine stripes or strips along the foliation, in millimeter-scale agglomerate crosscut foliation, or aggregated and distributed in agglomerates. When the alteration is strong, the rock foliation tends to disappear. Tourmalinization appears in two forms, one is symbiotic with altered biotite, and the other forms tourmaline clusters, veins or tourmaline quartz clusters and veins. Metal sulfides are usually filled among tourmaline grains or in mineral fractures, reflecting the relatively earlier formation of tourmaline.

3.5. Mineralization stage

Mineralization is closely related to shear belts, and ore bodies are controlled by belt zones. The shear belt evolves from ductile to brittle with changes in temperature and pressure during orogeny and dome uplift. Different evolution stages of shear belt correspond to different mineralization stages. At the disseminated-banded mineralization stage, micro-cracks and microstructures such as “C” foliations and grain boundary slip are developed, and metallogenic materials are initially enriched. Disseminated–banded mineralization or orebodies at this stage are foliated and parallel to current foliation, and correspond to streaks or banded alterations. The ore minerals are simple, mainly pyrrhotite, chalcopyrite and sphalerite, no pyrite. Except for the occasional ring pyrrhotite contained in chalcopyrite, there is no obvious inclusion or metasomatism among the metal sulfides, and the mineral formation sequence is not obvious.

At the massive–veined mineralization stage, interlayer fractures and various extensional fissures developed, and hydrothermal fluids filled and metasomatized along various structural fissures to form massive and veined ore bodies, corresponding to various forms of alteration. Various types of ores such as massive, breccia, disseminated, and veined were formed at this stage. The metasomatism is obvious, and the solid exsolution separation structure of sphalerite is common. The massive ores mainly consist of pyrrhotite, chalcopyrite and sphalerite, occasionally chalcocite and no pyrite. The wall rock breccias are common in the ores, which are metasomatism residues, with the quartz particles dissolved, and the pyrrhotite and sphalerite replaced by chalcopyrite. Pyrite occurs in quartz veined ores and altered rocks, and occasionally replaces pyrrhotite. Arsenopyrite is seen in agglomerate ore. This stage is the main metallogenic stage, superimposed on the previous stage to form rich ore bodies.

The mineralization stages and mineral formation sequence are shown in Fig. 7.

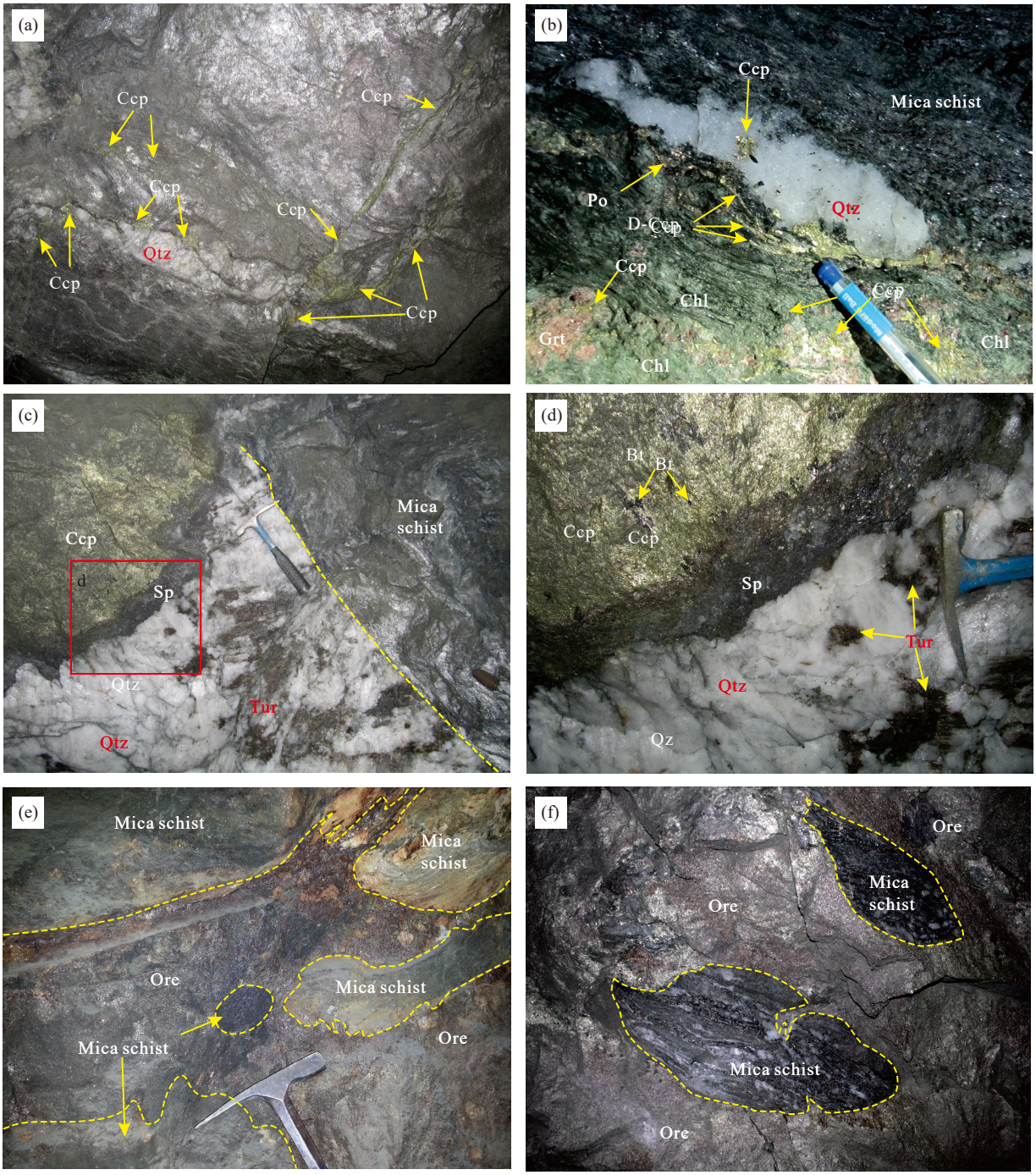

Fig. 5. Photographs taken in the adits from the Liwu copper deposit (after Zhou Q et al., 2017). a–banded sulfide ores and lenticular ore-bearing quartz veins on one side and several thin, clean sulfide veins on the other side; the former are parallel to the foliation of the wall rock, whereas the latter crosscut the foliation and the former. b–banded sulfide ores and ore-bearing quartz veins in a staurolite-garnet-mica schist. (c–d)–a clear crystallization sequence showing the veined tourmaline-quartz-chalcopyrite-sphalerite belt (early stage), veined sphalerite belt (middle stage) and massive chalcopyrite belt (late stage) from wall rock to orebodies. (e–f)–wall rock captured and surrounded by large veined and massive orebody. Abbreviations: Bt –biotite; Ccp –chalcopyrite; Chl –chlorite; Grt –garnet; Po –pyrrhotite; Qtz –quartz; Sp –sphalerite; Tur–tourmaline.

4. Sampling and analytical methods

4.1. Sampling

Samples of the sulfide ore-associated quartz-calcite-tourmaline veins at different mineralization stages were mainly collected from the Baixianglin and Zhongzui ore bolcks of the Liwu deposit, and prepared for fluid inclusion tests. Discriptions of these samples are presented as below.

4.1.1. Disseminated-band mineralization stage

Metallic sulfide-quartz veins: This type of mineralization occurs in layers in the Baixianglin disseminated-striped deposit. The quartz veins contain a lot of pyrrhotite, chalcopyrite and sphalerite, but without pyrite.

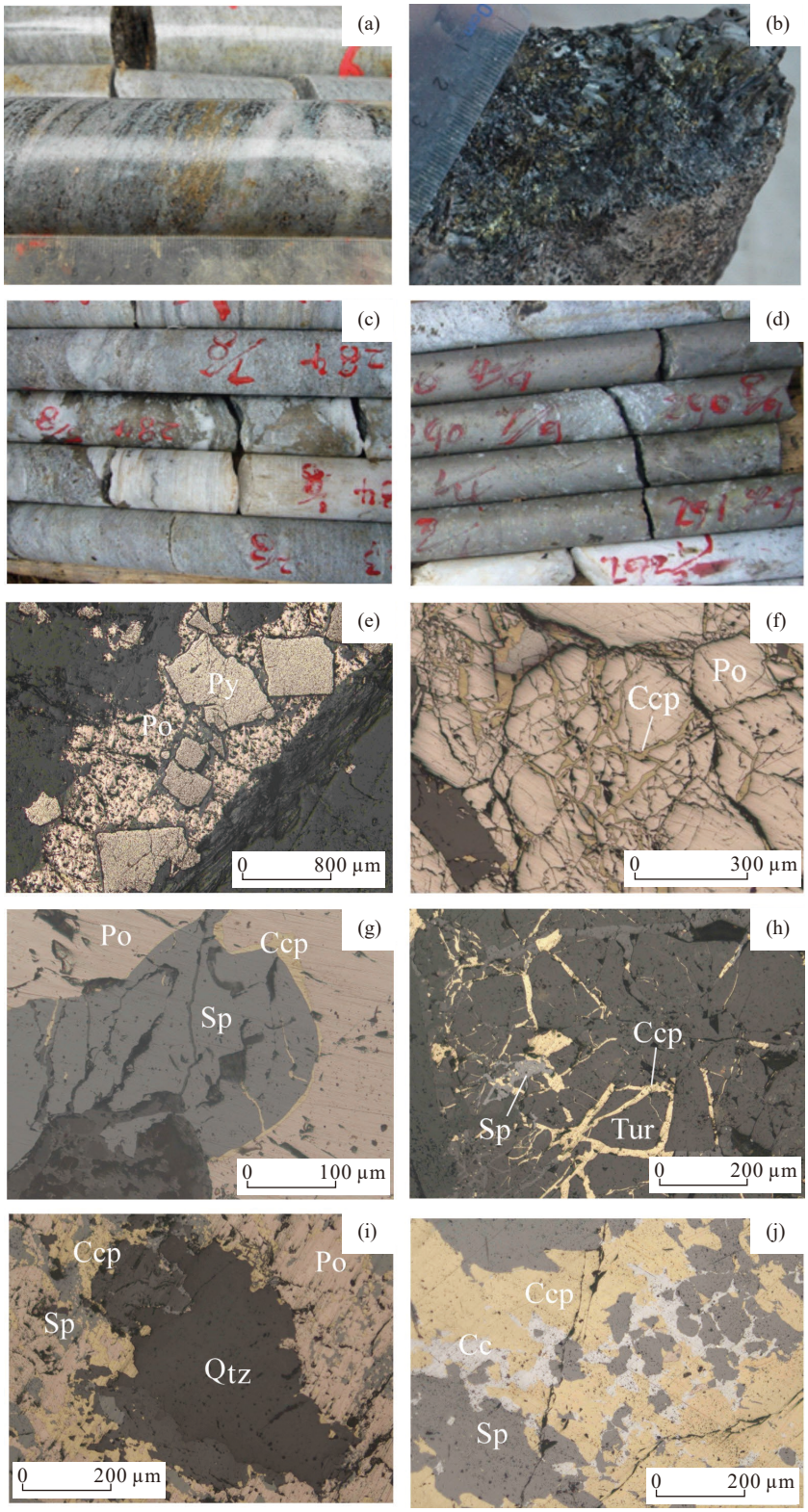

Fig. 6. Typical ore samples and photomicrographs of the Liwu copper deposit. a–disseminated-banded ore; b–tourmaline-bearing quartz vein-type ore; c–brecciated ore; d–massive ore; e–euhedral pyrite and anhedral pyrrhotite; f–chalcopyrite stockwork metasomatism along two groups of cracks of pyrrhotite; g–chalcocite metasomatism along sphalerite margin and fissure; h–sphalerite and chalcopyrite are deposited along tourmaline fissure and grain gap; i–quartz was metasomatized and etched by pyrrhotite, chalcopyrite, and sphalerite, etc; j–chalcocite was metasomatized by chalcopyrite and sphalerite. Cc–chalcocite; Ccp–chalcopyrite; Po–pyrrhotite; Py–pyrite; Qtz–quartz; Sp–sphalerite; Tur–tourmaline.

4.1.2. Massive-veined mineralization stage

Tourmaline-quartz-sulfide (vein): Tourmaline is formed slightly earlier than sulfides (Fig. 6h), and can be taken as the early stage of mineralization.

Metal sulfide-quartz (vein): Sulfide ore-associated quartz veins were collected near the rich ore body, which mostly

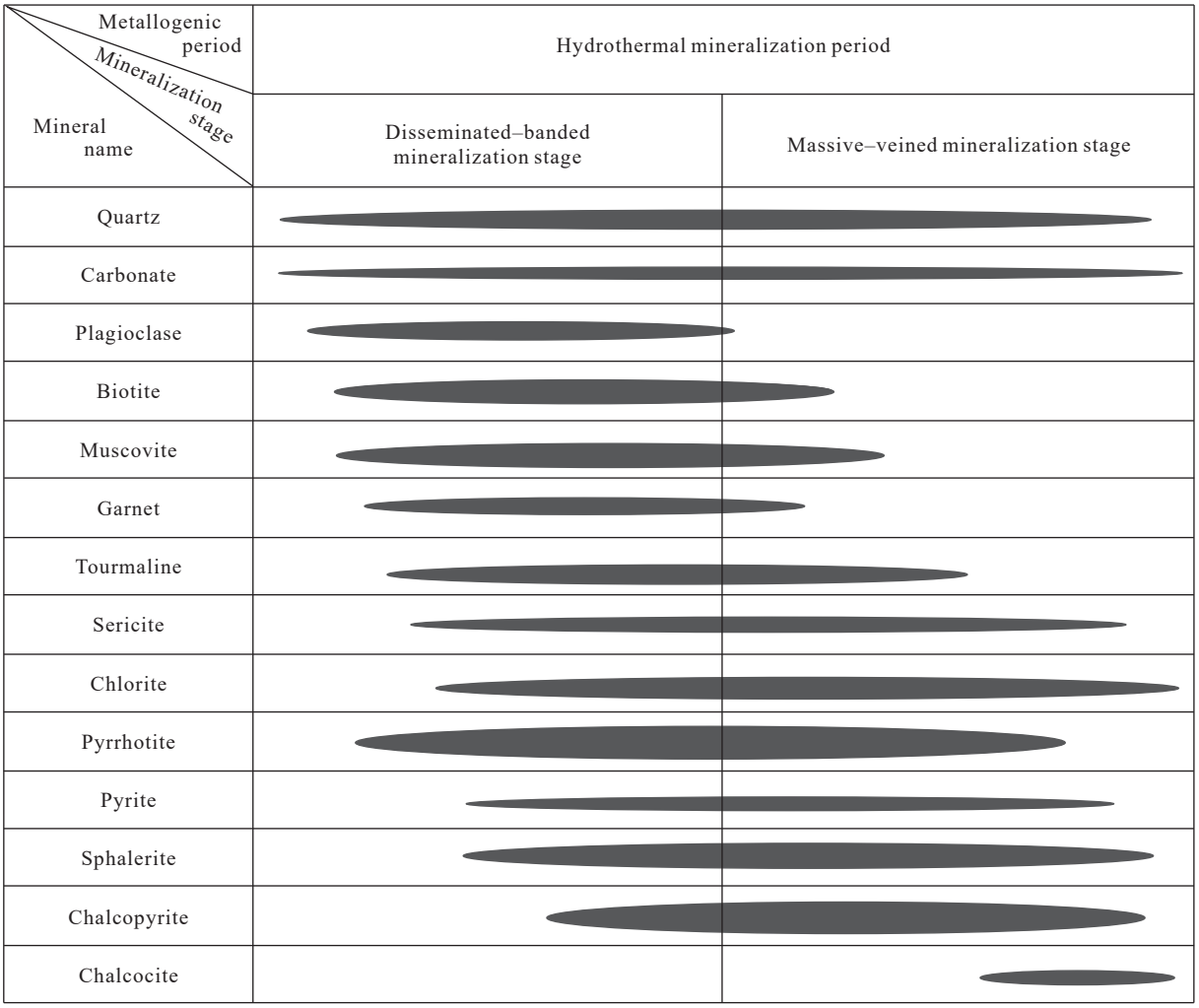

Fig. 7. Mineralization stages and mineral formation sequence of the Liwu copper deposit.

occur in bedding in the altered wall rocks or close to the ore body. Fluid inclusion test was carried out on the quartz, which represents the main stage of mineralization.

Quartz-calcite vein: This type of vein contains minor sulfide minerals, representing the late stage of mineralization. The calcite at this stage was selected for fluid inclusion tests.

4.2. Analytical methods

Petrographic observation and analysis of the fluid inclusions were carried out in the laboratory of Chengdu Center, China Geological Survey, and the instrument was a LeiCA DM4500P (Leica, Germany) microscope.

Qualitative determination for a single FI composition was performed using a Laser Raman spectrometer. The Ar^+ laser wavelength was mainly 514 nm, and laser power 40 mW, diameter of laser beam spot 1 μm was used in this study. During the measurement, the spectral resolution was 2 cm^{-1}, and the spectral range of 1200–1400 cm^{-1}, 2909–2920 cm^{-1} and 2320–2340 cm^{-1} was specially selected for CO_2, CH_4 and N_2 respectively.

Cooling and heating experiments of fluid inclusions therein were carried out by a Leica DM4500 petrographic microscope equipped with a Linkam THMSG600 heating/freezing stage. Microthermometry was calibrated using synthetic fluid inclusions. The uncertainties of the measurements are ±0.1°C for freezing and ±1°C for heating. Heating and cooling rates were controlled to be about 10°C per minute, and even reduced to 0.2°C to 1.0°C per minute near phase transformation temperature.

5. Results

5.1. Petrography of the fluid inclusions

Fluid inclusions mainly occur in quartz and subordinately occur in tourmaline at each stage. The shapes of fluid inclusions observed under the microscope are mainly ellipses, spindles, negative crystals and irregular shapes (Fig. 8). Most of them are star-shaped and group-banded, whereas some are isolated. Fluid inclusions distribute along the micro-cracks. Primary fluid inclusions and secondary fluid inclusions can be distinguished according to the petrography characteristics of fluid inclusions. The primary fluid inclusions are usually isolated and zonal. The secondary fluid inclusions are distributed linearly along the healed fissure and cut through the mineral crystals. The pseudo secondary inclusions are distributed linearly along the healed fissure, but could not cut

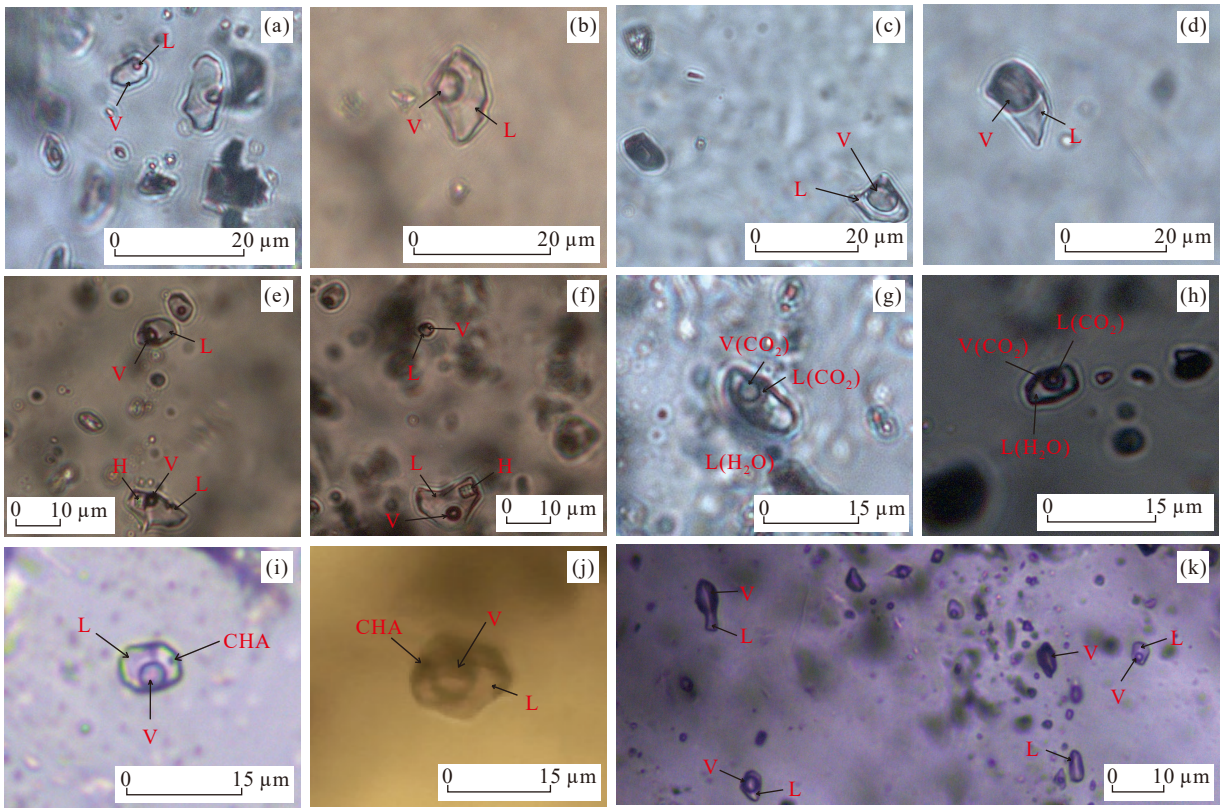

Fig. 8. Photomicrographs of fluid inclusions of the Liwu copper deposit.(a–b)–liquid two-phase inclusion; (c–d)–vapor two-phase inclusion; (e–f)–daughter mineral-bearing three-phase inclusion and liquid two-phase inclusion in the same microscopic field of view; (g–h)–CO_2-bearing three-phase inclusion; (i–j)–daughter mineral-bearing three-phase inclusion and the daughter mineral is chalcopyrite crystal; k–vapor two-phase inclusion, liquid two-phase inclusion, vapor fluid inclusion and liquid fluid inclusion in the same microscopic field of view.V–vapor phase; L–liquid phase; H–halite crystal; CHA–chalcopyrite crystal; L(H_2O)–liquid phase H_2O; V(CO_2)–vapor phase CO_2; L(CO_2)–liquid phase CO_2.

through the mineral crystals. Only the primary inclusions were selected for testing in this study. These inclusions can be divided into the following types, according to their composition, phase state at room temperature and phase change during the freezing and heating process.

(i) Liquid two-phase inclusions. The inclusions of this type show two-phases at room temperature, the gas-liquid ratio is less than 50%, and they are homogeneous as liquid phase when heated. The inclusions are distributed with scattered, banded and isolated shapes. The shape is oval, irregular, elongated, negative crystal and square. Their sizes mostly range from 3 μm to 20 μm, and reach 40 μm. Some of the inclusions contain CO_2 and CH_4, which can be seen in various mineralization stages. Some of them did not contain CO_2 and CH_4, and most of the inclusions were less than 10 μm, which mainly occur in calcite at the late stage.

(ii) Vapor two-phase inclusions. The inclusions of this type show two-phases at room temperature, the gas-liquid ratio is greater than 50%, and they are homogeneous as vapor phase when heated. This type of inclusion occurs both at the disseminated-banded mineralization stage and at the massive-veined metallogenic stage.

(iii) CO_2-bearing three-phase inclusions. This type of inclusion shows three-phases at room temperature, and its shape is oval, irregular, negative crystal, elongated, etc. Their sizes are mainly 4–20 μm, and some of them are larger than 30 μm. The inclusions contain CO_2 and CH_4. And they mainly occur at the massive-veined metallogenic stage.

(iv) Daughter mineral-bearing three-phase inclusions. The daughter minerals are chalcopyrite and halite daughter crystals. The formers mainly occur in tourmaline, and the latters occur at the massive-veined metallogenic stage.

(v) Vapor fluid inclusions. It shows a single-phase at room temperature, and occurs both at the disseminated-banded mineralization stage and at the massive-veined metallogenic stage.

(vi) Liquid fluid inclusions. Inclusions of a single liquid phase are also observed at the disseminated-banded and massive-veined metallogenic stages.

5.2. Microthermometry of the fluid inclusions

(i) Disseminated-band mineralization stage

Inclusions in the ore-associated quartz at this stage are irregularly developed and distributed in groups or in a single grain. These inclusions include two-phased inclusions containing CH_4 or CO_2-CH_4, single-phased inclusions containing CH_4 or CO_2, and pure H_2O inclusions. The gas-liquid ratios of the two-phased inclusions vary from 5 vol.% to 60 vol.%. The homogenization temperature of the inclusions is 181–375°C (Fig. 9a), with three peaks at 210–230°C, 310–330°C and 360–380°C, respectively; and the freezing point temperature is −13.1–−3.2°C. According to Bodnar's (1993) salinity-freezing point relationship table, its

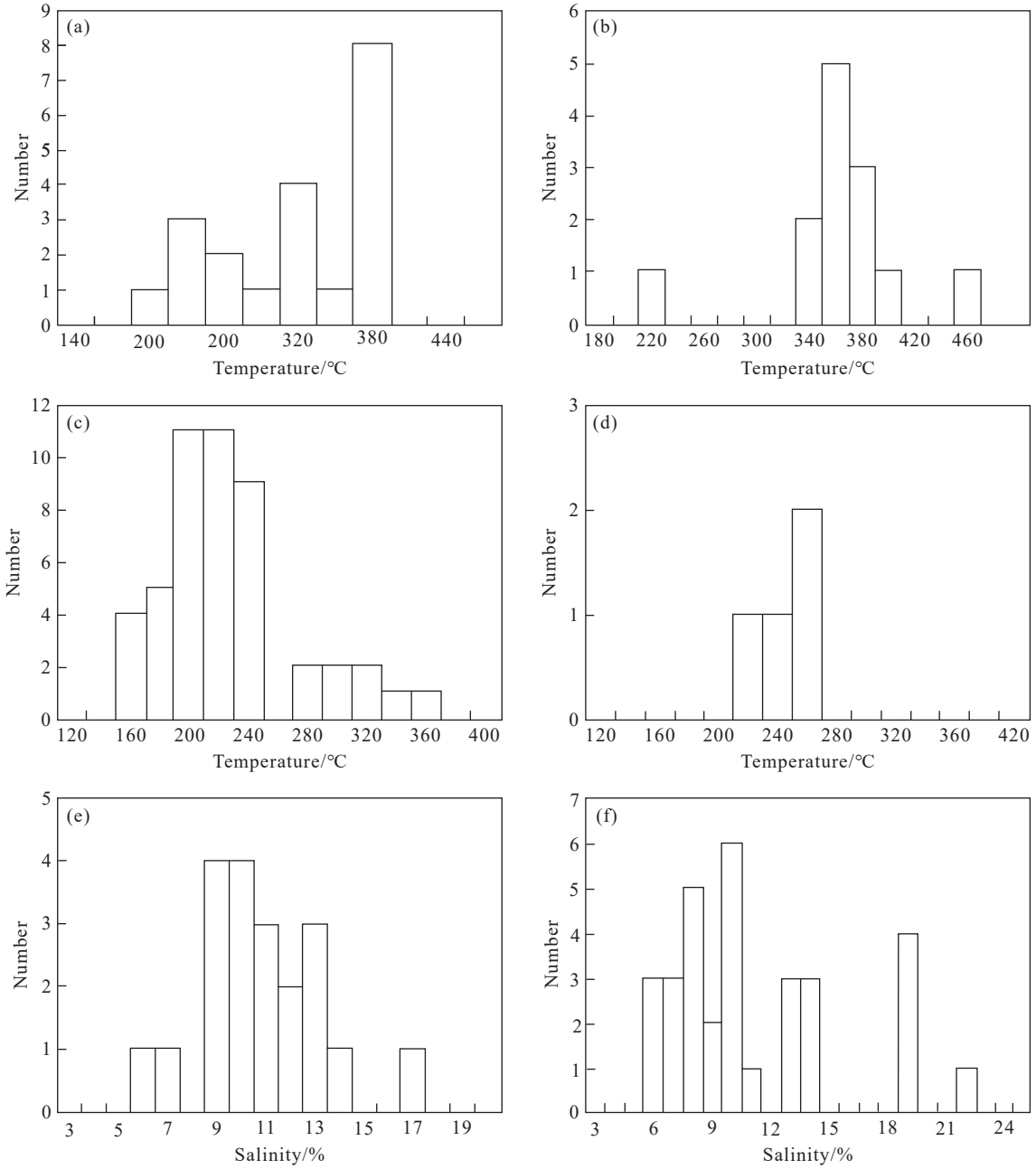

Fig. 9. Homogenization temperature and salinity of fluid inclusions at each stage.a–homogenization temperature at stage I; b–homogenization temperature at stage II; c–homogenization temperature at stage III; d–homogenization temperature at stage IV; e–salinity at stage I; f–salinity at stage III.

salinity is 5.26%–16.99% NaCl equiv., with a concentration of 9%–14% (Fig. 9e).

The two-phased inclusions that contain CH_4 with a gas-liquid ratio of 5–15 vol.% at this stage have a homogenization temperature of 181–301°C with an average of 246°C and a salinity of 8.41%–12.73%; The homogenization temperature of the inclusions that contain CH_4 and CO_2 with a gas-liquid ratio of 40–60 vol.% is between 317°C and 375°C, with an average of about 359°C, and with a salinity of 8.81%–16.99%.

(ii) Massive-veined mineralization stage

At tourmaline-quartz-sulfide stage (II), there are few inclusions in tourmaline, most of which are isolated or scattered, and locally occur in small groups. The two-phased inclusions mainly contain CH_4 plus minor CO_2; their size is mostly 4–15 μm with a gas-liquid ratio of 20–30 vol.%. However, some inclusions are gas (with a gas-liquid ratio of about 90 vol.%). In addition, a few three-phased inclusions of chalcopyrite sub-minerals are also observed, indicating that the fluid is rich in Cu-bearing mineral. The inclusions with a gas-liquid ratio of 20–30 vol.% show a homogenization temperature of 332–369°C (N=10); and homogenization temperatures of about 213°C and 390–450°C are also obtained for those inclusions with gas-liquid ratios of about 10 vol.% and 50 vol.%, respectively (Fig. 9b). The chalcopyrite sub-mineral inclusions with gas-liquid ratios of

20–50 vol.% have homogenization temperatures of 347–450°C. The melting temperature of the inclusion clathrate is 13.8–20.8°C. However, the salinity cannot be estimated by the melting temperature of the clathrate, due to the influence of CH_4.

At polymetallic sulfide-quartz stage (III), quartz is rich in inclusions, including two-phased inclusion that mainly contains CH_4 plus minor CO_2, two-phased or three-phased inclusion that contains CO_2 and CH_4. This stage of quartz also includes a single-phased CH_4-CO_2 inclusion, a salt daughter crystal inclusion and a single-phased H_2O inclusion. The two-phased inclusions that contain CH_4 plus minor CO_2 show a gas-liquid ratio of 5–10 vol.%, and a homogenization temperature of 142–343°C (Fig. 9c), with three peaks of 200–240°C, 260–290°C and 310–340°C, respectively. The freezing point temperature is −3.3–−18.3°C, and the calculated salinity is 5.41%–21.19% (Fig. 9f), with three intervals of 5%–10%, 12%–14% and 18%–19%, respectively.

The gas-liquid ratio of two-phased or three-phased inclusions containing CO_2 and CH_4 is mostly 10–30 vol.%, and the rich gas phase is mostly 50–60 vol.%. The homogenization temperature is 195–350°C, roughly distributed in three intervals of 200–250°C, 260–300°C, and 320–350°C. The temperature distribution is similar to that of two-phased inclusions containing CH_4 and a small amount of CO_2. The melting temperature of the clathrate is 5.6–14.7°C, which is greatly influenced by CH_4. The homogenization temperature of CO_2-CH_4 phased inclusions is 4.7–23.4°C.

At quartz-calcite stage (IV), there are few and small inclusions in calcite, mostly less than 10 μm, mainly two-phase inclusions containing H_2O and a very small amount of CH_4 and CO_2, the gas-liquid ratio is mostly 5–10 vol.%, and the homogenization temperature was measured at 230–268°C (Fig. 9d).

5.3. Compositions of the fluid inclusions

Raman components of all the types of inclusions at stages I–IV are analyzed in this study, and the results are shown in Fig. 10. The laser Raman analysis results are as follows.

At stage I, the two-phase inclusions (with a gas-liquid ratio of about 15 vol.%) are mainly composed of CH_4 in the gas phase, and contain minor H_2S, C_2H_4 and C_6H_6 (Fig. 10a). The gas phase components detected in the inclusions (with a gas-liquid ratio >40 vol.%) at this stage are mainly CH_4 and CO_2. The gas phase components of the inclusions (with a gas-liquid ratio of about 25 vol.%) in tourmaline at stage II are mainly CH_4 and H_2O, and contain minor CO_2 (Fig. 10b). In addition, three-phased inclusions that contain chalcopyrite daughter crystals are also observed (Fig. 10c), indicating that the fluid at this stage is rich in Cu. The gas phase components in phase III inclusions are mainly CH_4 and CO_2, some inclusions contain more CH_4 (with a gas-liquid ratio of 10 vol.%) (Fig. 10d), or more CO_2 (with a gas-liquid ratio of about 25 vol.%) (Fig. 10e). The single-phased inclusions at this stage (Fig. 10f) are mainly composed of CH_4 and CO_2, with a small amount of H_2O, N_2, H_2S and C_6H_6. The gas phase components of calcite inclusions (with a gas-liquid ratio of about 10 vol.%) at stage IV are CH_4, CO_2 and H_2O, and the contents of CH_4 and CO_2 become less (Fig. 10g–h). The H_2O peak in the liquid phase is flat at this stage, indicating a low salinity.

Results of Raman analysis show that the liquid phase composition of the inclusions is mainly H_2O plus minor CH_4 at stage I–II, and a small amount of CO_2 and CH_4 at stage III. The gas phase components of the inclusions are mainly CH_4 and CO_2, and contain minor N_2, H_2S, C_2H_4, C_6H_6 and H_2O. In addition, content of CH_4 decreased gradually from the early stage to the late stage, whereas the content of CO_2 gradually increased, and then decreased at stage IV.

The composition of fluid inclusions at different stages can be obtained by laser Raman analysis. However, its absolute content cannot be obtained, and the composition analysis of fluid inclusion groups can make up for this deficiency. In this paper, previous test data were collected and reanalyzed, and the component of inclusions was obtained (Table 1).

Composition data of the inclusion groups were mainly obtained by testing the ore containing quartz at stage III. As shown in Table 1, liquid of the inclusions mainly contains Na^+, K^+ and Ca^{2+} cations, and Cl^- anions with a low F^- content. A few inclusions contain relatively high SO_4^{2-}; however, the others are generally very little. These features indicate that the fluid is dominately Na^+- K^+ (Ca^{2+})-Cl^- rich, and subordinately Na^+- K^+ (Ca^{2+})-SO_4^{2-} rich. The pH of the inclusions is 6.6–6.8, suggesting that the fluid is slightly alkaline. Components of the gas phase are mainly H_2O, CO_2, CH_4 plus minor H_2. According to the research of Roedder (1971), composition parameters of liquid phase related to the magma or metamorphic hydrothermal fluids have a Na^+/K^+ ratio of <2 and a $Na^+/(Ca^{2+}+Mg^{2+})$ ratio of >4, whereas the hot brine has a Na^+/K^+ ratio of >2 and a $Na^+/(Ca^{2+}+Mg^{2+})$ ratio of <1.5. Atmospheric precipitation generally falls between the two end-members. Table 1 shows a Na^+/K^+ ratio of 0.52–70.44, most of which is larger than 2; and also shows a $Na^+/(Ca^{2+}+Mg^{2+})$ of 0.23–72.05, most of which is larger than 1.5. In conclusion, the composition parameters of the fluid inclusion do not show any single fluid characteristics, indicating that it may be a mixed fluid.

6. Discussion

6.1. Isotopic geochemistry

6.1.1. Hydrogen and oxygen isotopes

Previous studies reported hydrogen and oxygen isotopic data for the fluid inclusions of the ore-associated quartz at stage III (Song TH and Xing SC, 1990; Feng XL et al., 2008). Generally, $\delta^{18}O$ value ranges from −8.79‰ to 13.93‰, with an average of 0.58‰; and δD value ranges from −64.1‰ to −98.3‰ (mainly from −64.1‰ to −77.9‰), with an average of 34.2‰. Compared to the hydrogen and oxygen isotopic components of different types of water (Table 2), it can be found that they are in good agreement with the δD value of magmatic water; whereas a few samples also fall into the

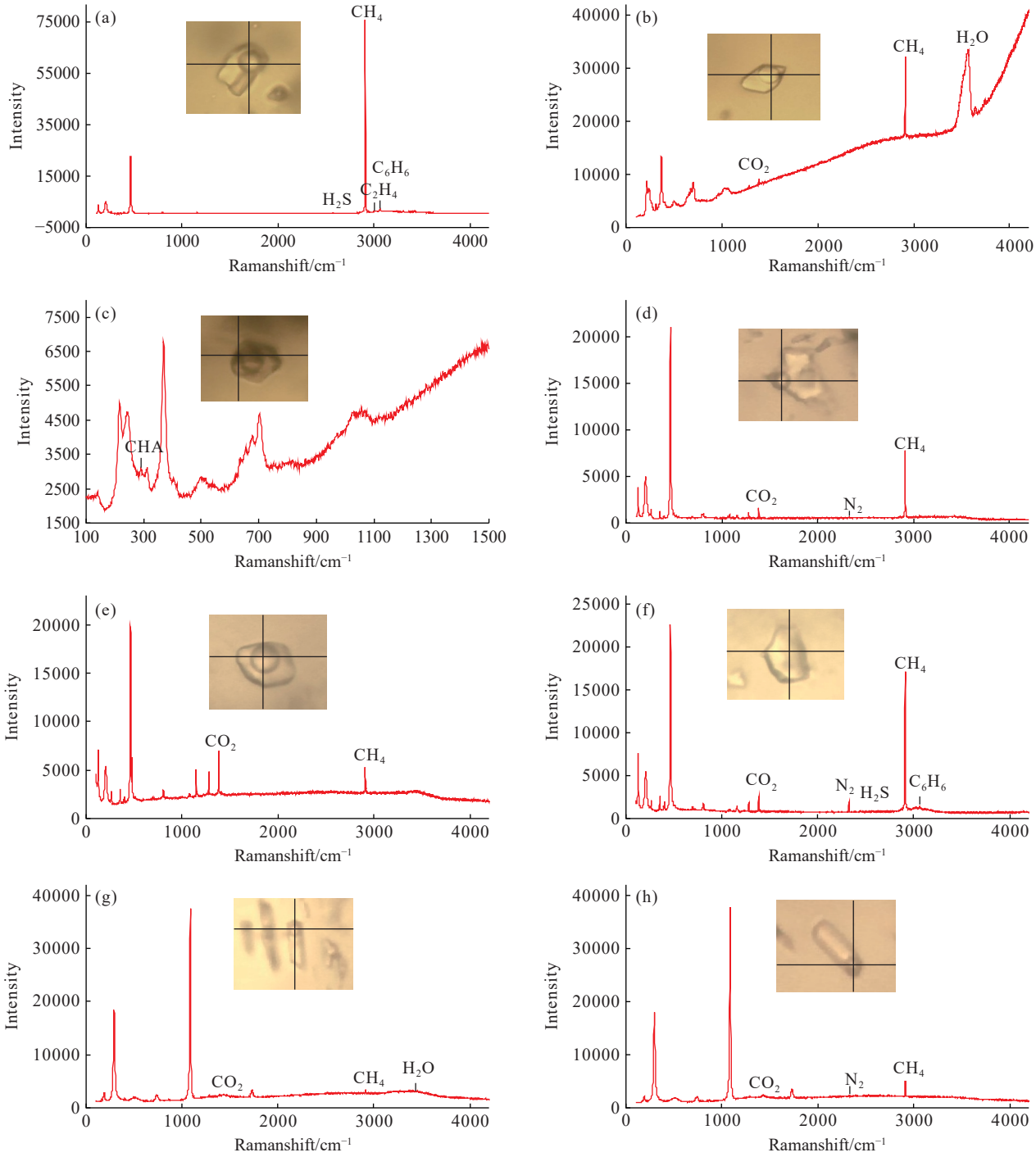

Fig. 10. Raman spectrum of inclusions. a–inclusions at stage I; (b–c)–inclusions at stage II; (d–f)–inclusions at stage III; (g–h)–inclusions at stage IV. CHA–chalcopyrite.

overlapping area between the magmatic water and the metamorphic water.

On the H-O diagram (Fig. 11), some samples are plotted close to magmatic water and metamorphic water, whereas a few samples are plotted close to the atmospheric precipitation line. All the samples are generally located between the magmatic water (metamorphic water) and the atmospheric precipitation, showing a trend shifting from the magmatic water (metamorphic water) to the atmospheric precipitation. Thus, the fluid at this stage should be a mixture of magmatic water (or metamorphic water) and atmospheric precipitation.

6.1.2. Sulfur isotope

Song HL et al. (1995) reported $\delta^{34}S$ values of −1.2‰–7.63‰ for pyrites in the surrounding rock, and $\delta^{34}S$ values of +2‰–+8.7‰ for the sulfide ores. Yao P et al. (2008, 2011) reported $\delta^{34}S$ values of +1‰–+9.83‰ for the disseminated sulfide ores, and $\delta^{34}S$ values of +5.2‰–+9.2‰ for the massive sulfide ores. The sulfur isotopes of the two types of ores are significantly different. At the disseminated mineralization stage, metal sulfides were disseminated and mineralized along the foliation of the altered schist, and the fluid and the surrounding rock underwent a strong water-rock

Table 1. Composition and parameters of the fluid inclusions.

Numberr	Sample serial number	Mineral name	Decrepitation temperature/ °C	Liquid composition/10^{-6}								Gas phase composition/10^{-6}					Ingredient parameters					
				K^+	Na^+	Ca^{2+}	Mg^{2+}	Li^+	F^-	Cl^-	SO_4^{2-}	HCO_3^-	pH	H_2O	CO_2	CO	CH_4	H_2	Na^+/K^+	$Na^+/(Ca^{2+}+Mg^{2+})$	Ca^{2+}/Mg^{2+}	F^-/Cl^-	SO_4^{2-}/Cl^-	CO_2/H_2O
1	JLLW01	quartz	100–600	0.84	12.07	0.61	0.029	0.005	0.11	16.78	0.00	0	6.8	471.85	187.25	0.50	0.07	0.22	14.37	18.89	21.03	0.007	0.000	0.40
2	JLLW16	quartz	100–600	0.30	0.44	0.36	0.005	0.005	0.09	1.55	0.00	0	6.6	201.55	112.30	0.05	0.04	0.17	1.47	1.21	72.00	0.058	0.000	0.56
3	JLLW17	quartz	100–600	0.10	5.31	0.14	0.019	0.010	0.05	6.90	0.00	0	6.6	325.33	172.55	0.25	0.03	0.18	53.10	33.40	7.37	0.007	0.000	0.53
4	JLLW18	quartz	100–600	0.18	3.23	0.84	0.005	0.005	0.08	5.01	0.05	0	6.6	318.25	158.65	0.25	0.04	0.16	17.94	3.82	168.00	0.016	0.010	0.50
5	JLLW19	quartz	100–600	0.09	6.34	0.05	0.038	0.005	0.00	7.65	0.05	0	6.6	444.32	136.58	0.50	0.03	0.15	70.44	72.05	1.32	0.000	0.007	0.31
6	JLLW21	quartz	100–600	1.08	5.33	0.32	0.534	0.010	0.07	7.02	2.50	0	6.6	402.31	172.25	0.50	0.03	0.15	4.94	6.24	0.60	0.010	0.356	0.43
7	JLWJG03	quartz	100–600	1.85	5.95	0.03	0.079	0.005	0.00	7.21	0.05	0	6.7	426.97	188.63	0.50	0.03	0.16	3.22	54.59	0.38	0.000	0.007	0.44
8	JLWJG06	quartz	100–600	0.37	0.63	0.72	0.004	0.005	0.05	1.25	0.00	0	6.6	389.58	101.25	0.05	0.03	0.17	1.70	0.87	180.00	0.040	0.000	0.26
9	JLHND01	quartz	100–600	0.33	1.24	0.05	0.001	0.005	0.00	2.58	0.00	0	6.6	333.55	171.56	0.25	0.02	0.11	3.76	24.31	50.00	0.000	0.000	0.51
10	JLBXL02	quartz	100–600	2.36	9.84	0.09	0.050	0.005	0.06	14.88	0.05	0	6.8	488.63	381.55	0.55	0.06	0.24	4.17	70.29	1.80	0.004	0.003	0.78
11	LB6	quartz	130–650	0.66	2.52	0.28	0.350	0.010	0.07	2.80	0.00	0	6.8	666.70	341.50	0.00	46.88	0.50	3.82	4.00	0.80	0.025	0.000	0.51
12	LB9	quartz	130–650	0.25	0.13	0.43	0.140	0.010	0.00	1.90	0.00	0	6.6	600.00	49.35	0.00	18.42	0.06	0.52	0.23	3.07	0.000	0.000	0.08
13	LB14	quartz	130–650	0.33	0.52	0.32	0.310	0.010	0.02	1.90	0.00	0	6.6	233.30	76.38	0.00	4.40	0.06	1.58	0.83	1.03	0.011	0.000	0.33
14	LB18	quartz	130–650	0.29	0.70	0.36	0.080	0.010	0.00	0.60	0.00	0	6.5	400.00	162.70	0.00	10.00	0.01	2.41	1.59	4.50	0.000	0.000	0.41
15	LB20	quartz	130–650	0.54	2.56	0.21	0.120	0.010	0.04	2.30	2.50	0	6.7	433.30	234.00	0.00	10.00	0.06	4.74	7.76	1.75	0.017	1.087	0.54
16	LB26	quartz	130–650	0.33	0.67	0.28	0.070	0.010	0.00	0.90	0.00	0	6.6	466.70	124.00	0.00	38.94	0.06	2.03	1.91	4.00	0.000	0.000	0.27

Notes: 1–10 component data comes from Feng XL (2008); 11–16 comes from Song HL (1995).

Table 2. Hydrogen and oxygen isotope values of different types of water.

Types of fluids in nature	$\delta^{18}O_{SMOW}$/‰	δD_{SMOW}/‰
Raw water	−13–9	0–−140
Magmatic water	6–9	−40–−80
Metamorphic water	5–25	−20–−65
Seawater	−0.5–0.3	0 (average)
Atmospheric precipitation (rain)	50–10	50–−350
Underground heated rainwater	−16–3	25–−120
Volcanic rock, Pluton	5.5–10	−50–−90
Marine carbonatite	22–30	
Freshwater Carbonatite	18–25	

Notes: The numerical range is based on Lu WC (1986).

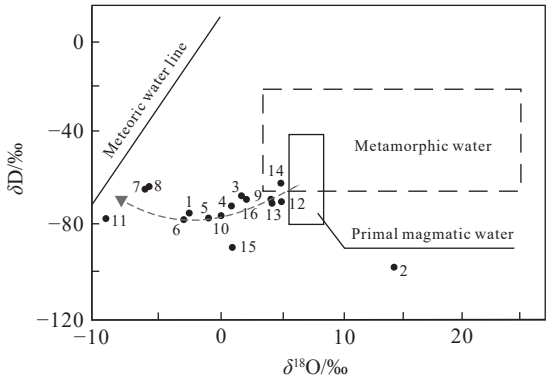

Fig. 11. Diagram of $\delta D-\delta^{18}O$ isotopes in fluid inclusions of ore-bearing quartz (Data from Song TH and Xing SC, 1990 and Feng XL et al., 2008).

reaction. During this process, a large amount of material from the surrounding rock was extracted into the fluids. As a result, its $\delta^{34}S$ value is relatively scattered, and similar to those of the surrounding rock. The massive mineralization was formed at stage IV, and metal minerals were filled and metasomatized in the relatively narrow space of the interlayer fracture zone. Sulfur from the surrounding rock at this stage was relatively few, and the $\delta^{34}S$ value was relatively concentrated, reflecting a similar component of the original fluid.

$\delta^{34}S$ value of the massive ore is +5.2‰–+9.2‰, which is obviously different from the surrounding rock. Other possible sulfur sources in the mining area are mantle sources (or basic rocks) and potential felsic rocks underneath the Jianglang dome. $\delta^{34}S$ value of the mantle source (or basic rock) is generally close to zero, which is inconsistent with those of the Liwu sulfide ores; accordingly, the mantle source can be precluded for the ore-froming source of Liwu copper deposit. The felsic intrusive rocks have $\delta^{34}S$ values varying from −13.4‰ to +26.7‰. In addition, the granite formed by re-melting of the crust commonly has a higher $\delta^{34}S$ value. In fact, the felsic intrusive rocks such as the Wenjiaping granite in this area were derived by partial melting of the lower crust (Liu J et al., 2022), and are very likely to be a sulfur contributor to the Liwu copper deposit.

6.2. Properties of the ore-forming fluids

The fluid mineralization in this area is accompanied by the

whole evolution process of the shear zone. During the process of regional orogeny and dome uplift, the shear zone was continuously raised from deep to shallow, the pressure gradually decreased, and it experienced ductile, ductile-brittle and brittle stages. According to the evolution process of the shear zone, the fluid mineralization stages can be divided. At the transition stage of shear band ductility to ductile-brittleness, the fluid goes through stage I; from the brittle-ductile to brittle transition stage in the shear zone, the fluid has experienced stages II, III and IV.

At stage I, dissemination-banded mineralization occurred along the mylonite plane, when the ore-forming fluid was a H_2O-NaCl-CH_4(-CO_2) system, the homogenization temperature was mainly 210–375°C, and the salinity was 5.26%–16.99%. At stage II, tourmaline occurred, when the fluid system was H_2O-NaCl-CH_4-CO_2, the homogenization temperature was concentrated at 332–369°C, and the Raman spectrum showed that its salinity was high. At stage III, rich ore-bodies were deposited, the fluid was a H_2O-NaCl-CO_2-CH_4 system, the homogenization temperature was mainly 200–350°C, and the salinity was 5.41%–21.19%. At stage IV, the quartz-calcite network veins were filled in the extensional fractures; the CO_2 and CH_4 contents in the fluid were greatly reduced; the homogenization temperature was 230–268°C, and the Raman spectrum shows that the salinity was low.

The fluid temporally changed from a H_2O-NaCl-CH_4(-CO_2) system to a H_2O-NaCl-CH_4-CO_2 system, and finally to a H_2O-NaCl system. The fluid temperature and salinity firstly increased and then decreased, the CH_4 content gradually decreased, and the CO_2 content firstly increased and then decreased. The volatile components in late calcite were greatly reduced.

6.3. Pressure and depth of the ore-forming fluids

The fluid pressure (P) is a function of the homogenization temperature (T_h) and the fluid salinity (ω). The empirical formula of Shao JL (1988) was used to calculate the pressure of two-phase fluid inclusion: $P=P_0\times T_h/T_0$ (where T_0=374+9.20ω; P_0=219+26.20ω; ω stands for salinity). After obtaining the pressure data, the metallogenic depth was estimated by referring to Sun FY et al. (2020). The fluid pressure of the stage I is 19.1–45.5 MP, and the ore-forming depth is estimated to be 1.9–4.6 km. The fluid pressure of stage Ⅲ is 14.3–36.1 MP, and the metallogenic depth is estimated to be 1.5–3.7 km.

6.4. Ore-forming fluid source and metallogenic mechanism

Fluid mixing, water-rock reaction, fluid boiling and phase separation are the main mechanisms for the precipitation of ore-forming minerals in hydrothermal deposits (Lu HZ et al., 2004; Li WB et al., 2007; Wu KW et al., 2008; Zhou H et al., 2013; Jiang YH et al., 2013; Wang J et al., 2013; Chen SY et al., 2013; Chen MH et al., 2013). Stages I and III are two metallogenic stages in this area. According to their inclusion characteristics, composition analysis and temperature measurement results, the two fluid precipitation mechanisms are different.

The Raman composition at stage I shows that the gas-phase composition of the liquid inclusions (with a gas-liquid ratio of 5–30 vol.%) is mainly CH_4, without CO_2. However, in the inclusions with a gas-liquid ratio larger than 40%, the gas-phase composition contains a large amount of CH_4 and CO_2, and the composition is obviously different from that of the formers. The temperature measurement of the inclusions shows that the homogenization temperature of the inclusions containing CH_4 (with a gas-liquid ratio of 5%–15%) is 181–301°C, with an average of 246°C and a salinity of 8.41%–12.73%; The homogenization temperature of the inclusions containing CO_2 and CH_4 (with a gas-liquid ratio of 40–60 vol.%) is 317–375°C, the average is 359°C, and the salinity is mainly 8.81%–16.99%. The two types of inclusions are also significantly different in homogenization temperature and related salinity. The testing results above show that the fluids captured at stage I have two components with different temperature and composition. The former belongs to a medium-temperature, low-salinity, CH_4-containing salt aqueous fluid, and the latter belongs to a high-temperature, medium-salinity, CH_4-CO_2 volatile fluid. The homogenization temperature and salinity of the volatile fluid is obviously higher than that of the brine fluid. These features indicate that the fluid did not boil at this stage (Pan XF and Liu W, 2006). In fact, fluid mixing was likely to have taken place, adding into a high temperature, high salinity and volatile fluid. Combined with this stage of mineralization accompanied by extensive wall rock alteration, the fluid precipitation mechanism should be both a fluid mixing and a water-rock reaction.

Raman analysis of stage III inclusions show that the composition of all types of inclusions is different in content, but the composition type is similar. The homogenization temperature of the two-phased inclusions containing CH_4 and a small amount of CO_2 are roughly similar to that of the two-phased or three-phased inclusions containing CH_4 and CO_2; the coexistence of daughter mineral-bearing inclusions, liquid inclusions and vapor inclusions were observed in the same microscopic field. These characteristics indicate that the fluid boiling occurred at this stage. Generally, boiling occurred in a small range, and its mineralization should be characterized by large intensity, small range and high grade (Zhang DH, 1997). The mineralization of stage III was the formation of massive ore-bodies by filling and metasomatism in the interlayer fracture zone, which was consistent with the features of boiling mineralization. In summary, the fluid precipitation mechanism at this stage should be fluid boiling.

Different fluid characteristics at each stage indicate that the source and properties of the fluid might be different. Stage I shows two fluid types. One of the fluids was formed by ductile shearing, with a medium-temperature, low-salinity, CH_4-containing and salt feature. CH_4 might be derive from the decomposition of organic matter or the related reaction of graphite. At the same time, a large amount of another high

temperature, medium salinity and CH_4-CO_2 volatile fluid was added. Considering that CO_2 content gradually dominated at stages II and III, this kind of high temperature, medium salinity and CH_4-CO_2 rich volatile fluid should gradually become the dominant fluid. The hydrogen and oxygen isotope data obtained at stage III show that the fluid δD value is very consistent with that of the magmatic water. Furthermore, a few samples fall into the overlapping area of magmatic water and metamorphic water. The δ^{18}O values are mostly close to magmatic water, but partially drift to the atmospheric water. Combined with the characteristics of hydrogen and oxygen isotopes and fluid characteristics, the other fluid at stage I might be from the magmatic water, which was added to the original metamorphic fluid and became the main fluid at stages II and III; whereas the atmospheric water was added in the ore-forming fluids at stage III. At stage IV, the fluids acted on the brittle stage of the shear zone, and the volatile components in the fluid were greatly reduced. The fluid were characterized by medium-low temperature and low salinity, which might be dominated by the atmospheric water.

6.5. Origin of the Liwu copper deposit

Different stages of fluid mineralization were formed by magmatism and shear zone evolution. Metamorphic fluids of stage I joined magmatic fluids, and fluid mixing and extensive water-rock reactions resulted in the disseminated-striped mineralization. At stage III, magmatic fluids were dominant, and atmospheric water was added, the fluid boiling occurred, forming massive rich ore bodies.

The sulfur isotope of the Liwu copper deposit shows that δ^{34}S value of the disseminated ore sulfides at stage I is +1‰–+ 9.83‰, close to that of the surrounding rock (−1.2‰–7.63‰), indicating that more materials were extracted from the surrounding rock. δ^{34}S value of stage III massive ore minerals is +5.2‰–+9.2‰, similar to that of the magma, indicating a contribution of magma to the ore-forming materials. Hydrogen and oxygen isotopes show that the stage III is dominated by a magmatic water with the addition of an atmospheric water.

According to the review, the ore-forming fluid of the deposit has the characteristics of long-term, multi-stage and multi-source, and the ore-forming materials also have multiple sources. Mineralization is closely related to the evolution of shear zones, which are both ore-controling and ore-hosting structures for the Liwu copper deposit. In summary, the deposit belongs to a medium-high temperature hydrothermal deposit related to magmatism, and was controlled by the ore-hosting shear zones.

7. Conclusions

(i) Laser Raman analysis shows that the ore-forming fluid is a H_2O-NaCl-CH_4-CO_2 system. The microscopic thermometry of fluid inclusions shows that there are two mineralization stages, a dissemination-band mineralization stage with an homogenization temperature of 181–375°C and a salinity of 5.26%–16.99%, and a massive-veined mineralization stage with a homogenization temperature of 142–343°C and a salinity of 5.41%–21.19%. The ore-forming fluid is characterized by medium-high temperature and medium-salinity. The fluid precipitation mechanism at the dissemination-banded mineralization stage is fluid mixing and water-rock reaction, whereas the fluid precipitation mechanism in the massive-veined mineralization stage is fluid boiling.

(ii) The data of H-O isotope and S isotope from previous tests were collected, and the δ^{18}O values range from −8.79‰ to 13.93‰, with an average of 0.58‰. The δD values range from −64.1‰ to −98.3‰, with an average of 34.2‰. The δ^{34}S value of the disseminated ore sulfides is +1‰–+9.83‰, and that of the massive ore sulfides is +5.2‰–+9.2‰. δ^{34}S value of the disseminated ore sulfides is close to that of pyrite in the surrounding rock, indicating that more surrounding rock materials were added at this stage. δ^{34}S value of the massive ore sulfides at the massive-veined mineralization stage has similar sulfur isotope to that of the magmatic rocks, indicating a contribution of magma to the metallogenic materials. Hydrogen and oxygen isotopes indicate that the massive-veined mineralization stage is dominated by the magmatic water, with an addition of atmospheric water.

(iii) The ore-forming fluids of the ore deposit are characterized by long-term, multi-stages and multi-sources; and the ore-forming sources are also various. Cu-Zn polymetallic mineralization is closely related to the evolution of shear zones, which are the ore-controlling and ore-hosting structures in the ore deposits. The Liwu copper deposit is a medium-high temperature hydrothermal deposit related to magmatism and controlled by shear zones.

CRediT authorship contribution statement

Hua-yun Yuan, Qing Zhou and Yuan-bao Song conceived of the presented idea. Hua-yun Yuan, Qing Zhou, Hui-hua Zhang, Tong-zhu Li, Chang-nan Wang and Gao-lin Tang carried out field investigation. Hua-yun Yuan carried out the experiment. All authors discussed the results and contributed to the final manuscript.

Declaration of competing interest

The authors declare no conflicts of interest.

Acknowledgement

This work was financially supported by National Natural Science Foundation of China (42272106, 41202067), Open Fund of State Key Laboratory for Mineral Deposits Research, Nanjing University (2019-LAMD-K12), and China Geological Survey (DD20211386, DD20211392, DD20179603). We are grateful to Jin Liang, Nian-Liang Liu and Xue-Wen Tang from the Liwu Copper Co. Ltd., China, for their assistance in the field. In addition, special thanks are given to the anonymous reviewers for their nice suggestions.

References

Chen BL, Dong FX, Li ZJ. 1999. Ore-forming Model of Ductile Shear Zone Type Gold Deposits. Geological Review, 45(2), 186–192 (in Chinese with English abstract).

Chen MH, Zhu XP, Feng XL, Ding J, Yao P, Ma DF, Tang GL. 2013. Mineralizing fluids and genesis of the Heiniudong copper deposit in the Liwu copper orefield, Sichuan. Sedimentary Geology and Tethyan Geology, 33(1), 99–105 (in Chinese with English abstract).

Chen SY, Gu XX, Cheng WB, Zhen G, Han SY, Pen YW. 2013. Characteristics of ore-forming fluid and mineralization process of the Yangla copper deposit, Yunnan. Earth Science Frontiers, 20(1), 82–91 (in Chinese with English abstract).

Chen YJ, Ni P, Fan HR, F Pirajno, Lai Y, Su WC, Zhang H. 2007. Diagnostic fluid inclusions of different types hydrothermal gold deposits. Acta Petrologica Sinica, 23(9), 2085–2108 (in Chinese with English abstract).

Feng XL, Liu YS, Zhang HH, Wu ZB, Li TZ. 2008. Quartz inclusions from the ore-bearing rocks in the Liwu copper deposit, Jiulong, Sichuan. Sedimentary Geology and Tethyan Geology, 28(2), 1–11 (in Chinese with English abstract).

Ghazi AM, Vanko DA, RuizJ. 1994. Trace and rare element analysis in single fluid inclusions: an application of laser ablation ICP-MS. EQS, 75(44), 695.

Guo CY, Zhang WZ, Ge LS, Gao BF, Xia R. 2011. Several questions on tracing ore forming fluid by using hydrogen and oxygen isotope system. Journal of Mineralogy and Petrology, 31(3), 41–47 (in Chinese with English abstract).

Hu RQ, Yang MZ, Liang J, Liu Q, Lv HJ. 2018. Prospecting methods in the depth and peripheral region of the Liwu Cu-Zn deposit in Jiulong, Sichuan. Acta Geologica Sichuan, 38(02), 216–220 (in Chinese with English abstract). doi: 10.3969/j.issn.1006-0995.2018.02.008.

Jiang YH, Luo Y, Niu HC, Guo SL, Li NB. 2013. Study on fluid inclusions from the Luojiahe copper deposit in Zhongtiaoshan region. Acta Petrologica Sinica, 29(7), 2583–2592 (in Chinese with English abstract).

Li JZ, Liu YP, Shen ZW, Ma GT, Zhu XP, Tang GL, 2012. Geological characteristics, genesis and metallogenic time of the Heiniudong copper-zinc deposit in Jiulong county, Sichuan province. Acta Geologica Sinica 86, 1972–1993 (in Chinese with English abstract).

Li WB, Lai Y, Sun XW, Wang BG. 2007. Fluid inclusion study of the Bainaimiao Cu-Au deposit in Inner Mongolia, China. Acta Petrologica Sinica, 23(9), 2165–2176 (in Chinese with English abstract).

Liu J, Li WC, Zhou Q, Zhang HH, Li TZ, Dai YP, Shen ZW, Tang GL, Wang CN. 2022. Late Jurassic Wenjiaping high Sr/Y granite: A product of partial melting of the Precambrian basement rocks trigged by lithospheric extension in the Songpan–Garzê fold belt, SW China. Geological Journal, 57(10), 4370–4387. doi: 10.1002/gj.4554.

Lu HZ, Fan HR, Ni P, et al. 2004. Fluid Inclusions. Beijing, Scientifical Press (in Chinese).

Lu HZ, Guo DJ. 2000. Progress and Trends of Researches on Fluid Inclusions. Geological Review, 46(4), 385–392 (in Chinese with English abstract).

Lu HZ, Guy Arcambault, Li YS, Wei JX, Chen NN, Zhang GP, Yuan WC, Chen XB, Long HB. 1999. The Relation between Deformation Types and Gold mineralization in the Linglong-Jiaojia District, Shandong Province, China. Acta Geologica Sinica, 73(2), 174–188 (in Chinese with English abstract).

Lu WC. 1986. Stable Isotope Geochemistry. Chengdu, Chengdu University of Geology (in Chinese).

Pan XF, Liu W. 2006. Fluid inclusions characteristics and ore-forming evolution of Jinwozi gold deposit. Acta Petrologica Sinica, 22(1), 253–263 (in Chinese with English abstract).

Roedder E. 1971. Fluid inclusion studies on the porphyry-type ore deposits at Bingham. Utah, Butte, Montana, and Climax, Colorado. Economic Geology, 66, 98–120.

Shao JL, 1988. Gold mine prospecting mineralogy. Wuhan, China University of Geosciences Press, 1–256 (in Chinese).

Song HL, Tian JY, Yan DP, et al. 1995. Deformation and metamorphism of the Jianglang metamorphic core complex in the western margin of the Yangtze Platform and the metallogenic model of the Liwu-type copper deposit. China University of Geosciences, Team 404 of Sichuan Geological Bureau (in Chinese).

Song TH, Xing SC. 1990. Discussion on Genesis of Liwu Copper Deposit. Southwest Deposit Geology, 4(4), 1–12 (in Chinese with English abstract).

Sun FY, Wang R, Wang YC, Li SD, Wang KY, Shi KT, Sun QF, Wang WY. 2020. Origin, Evolution of Ore-Forming Fluids and Metallogenic Mechanism of Nianzigou Molybdenum Deposit, Inner Mongolia. Journal of Jilin University (Earth Science Edition), 50(3), 768–780 (in Chinese with English abstract). doi: 10. 13278/j.cnkijj uese.20190121.

Wang J, Li BL, Zhang H, Xu QL. 2013. Evolution characteristics of Tongkuangyu copper fluid in the Zhongtiaoshan mountains, Shanxi Province. Global Geology, 32(2), 200–211 (in Chinese with English abstract).

Wang ZC, Liu JM, Liu HT, Zeng QD, Zhang S, Wang YB. 2010. Complexity and uncertainty of tracing fluid sources by means of H-O, C, S, N isotope systems: A case study of orogenic lode gold deposits. Acta Petrologica Et Mineralogica, 29(5), 577–590 (in Chinese with English abstract).

Wu KW, Zhong H, Zhu WG, Len CB, Gou TZ. 2008. Study on Ore-forming fluid of the Dahongshan stratiform copper deposit, Yunnan, China. Acta Petrologica Sinica, 24(9), 2045–57 (in Chinese with English abstract).

Yan DP, Zhou MF, Song HL, Fu ZR, Sun M. 2003. Tectonic controls on the formation of the Liwu Cu-rich sulfide deposit in the Jianglang Dome, SW China. Resource Geology 53, 89–100. doi: 10.1111/j.1751-3928.2003.tb00161.x.

Yao, JD. 1990. Genesis of the Liwu copper deposit. Acta Geologica Sichuan 10, 251–258 (in Chinese with English abstract).

Yao P, et al. 2011. Summary and Research Report on Typical Deposits of Liwu Copper Deposit. Chengdu Institute of Geology and Mineral Resources (in Chinese with English abstract).

Yao P, Wang MJ, Li JZ, Ma GT, Zhu XP. 2008. Isotopic Tracing of the Liwu-type Cu Deposits and Its Ore-forming Geological Significance. Acta Geoscientica Sinica, 19(6), 691–696 (in Chinese with English abstract).

Zhang DH. 1997. Overview of research on the ore depositional mechanisms in ore-forming fluid. Geological Science and Technology Information, 16(3), 53–58 (in Chinese with English abstract).

Zhang HH, Feng XL, Tang GL, Zhou Q, Li TZ, Zhu XP, Wu ZB, Xia XB. 2013. Structure Types and Mineralization in the Zhongzui Copper Deposit, Jiulong County, Sichuan Province. Geological Journal of China Universities, 19(1), 95–108 (in Chinese with English abstract).

Zhou H, Xi AH, Xiong YX, Liu JY, Yuan D. 2013. Progress in the Research on Fluid Inclusions. Acta Mineralogica Sinica, 33(1), 92–100 (in Chinese with English abstract).

Zhou Q, Li WC, Zhang HH, Li TZ, Yuan HY, Feng XL, Li C, Liao ZW, Wang SW. 2017. Post-magmatic Hydrothermal Origin of the Liwu Stratiform Copper Deposits, Western China: Direct Chalcopyrite Re-Os Dating and Pb-B Isotopic Constraints. Ore Geology Reviews, 89, 526–543. doi: 10.1016/j.oregeorev.2017.07.008.